SCIENCE CHINA
Information Sciences

• RESEARCH PAPER •

October 2020, Vol. 63 202306:1–202306:12
https://doi.org/10.1007/s11432-019-2850-3

Support vector machine based machine learning method for GS 8QAM constellation classification in seamless integrated fiber and visible light communication system

Wenqing NIU, Yinaer HA & Nan CHI*

Key Laboratory for Information Science of Electromagnetic Waves (MoE), Fudan University, Shanghai 200433*, China*

Received 5 September 2019/Revised 11 November 2019/Accepted 25 March 2020/Published online 21 September 2020

Abstract Visible light communication (VLC) network over optical fiber has become a potential candidate in ultra-high speed indoor wireless communication. To mitigate signal distortion accumulated in optical fiber and VLC channel, we present to utilize support vector machine (SVM) for constellation classification in two kinds of geometrically-shaped 8QAM (quadrature amplitude modulation) seamless integrated fiber and VLC system. We introduce 4 sub-bands to simulate multi-user. Experimental results show that system performance can be significantly improved, and transmission at -2.5 dBm input optical power under 7% forward error correction (FEC) threshold can be realized employing Circular $(7, 1)$ geometrically-shaped 8QAM and SVM. At overall capacity of 960 Mbps, Q-factor increases by up to 11.5 dB.

Keywords visible light communication, VLC, support vector machine, SVM, geometrically shaping, GS, VLC network, constellation classification

Citation Niu W Q, Ha Y, Chi N. Support vector machine based machine learning method for GS 8QAM constellation classification in seamless integrated fiber and visible light communication system. Sci China Inf Sci, 2020, 63(10): 202306, https://doi.org/10.1007/s11432-019-2850-3

1 Introduction

Nowadays, there has been consistent growth in the demand of communication system with higher data rate. Visible light communication (VLC) is an emerging field of optical communication which has advantages of high capacity, environment-friendly and anti-electromagnetic interference [1]. Additionally, it can be combined with illumination, and thus VLC is an ideal candidate for high-speed indoor wireless access [2] in future 5G and even 6G systems. Extensive researches that focus on VLC network have been done [2–11]. VLC network based on power-line communications (PLC) is investigated in [4, 5], but owing to the inherent characteristic of PLC, the data rate is not satisfactory. As optical fiber can provide huge modulation bandwidth and existing optical distribution networks can be reused [3], VLC network over optical fiber is a better solution. For high capacity VLC system, the severe bandwidth limitation introduced by light-emitting diode (LED) is a major bottleneck [12]. Multi-band quadrature amplitude modulation (QAM), where the signal is divided into several sub-bands for each user in the network, could support multiple access simultaneously, and the spectrum efficiency could be improved. Figure 1 is the overview of optical fiber-based VLC network. The multi-band data for different VLC access points (VAP) is firstly modulated at the central office, and then transmitted through fiber link. After split by optical

* Corresponding author (email: nanchi@fudan.edu.cn)

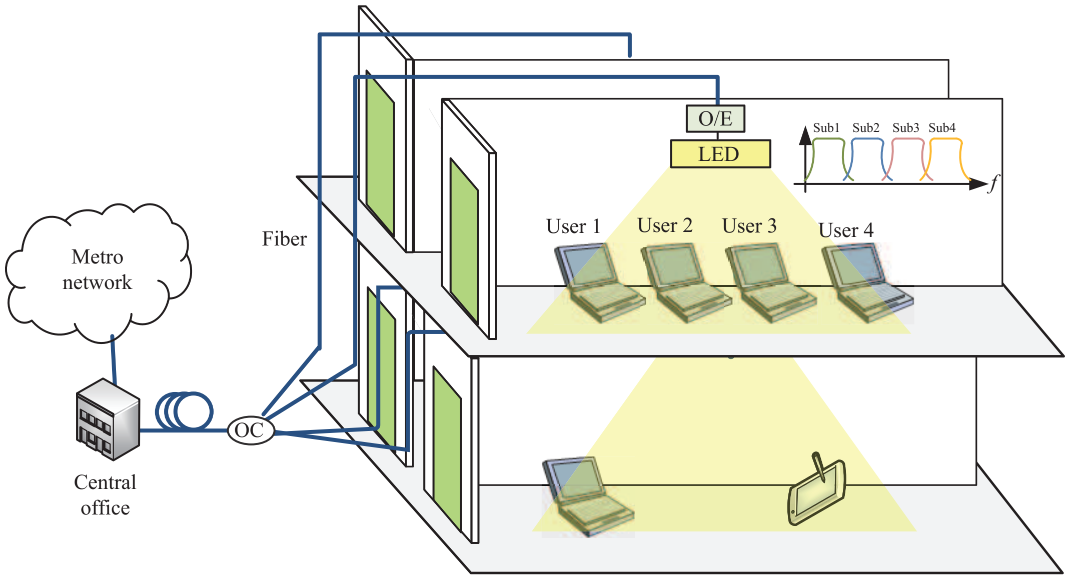

Figure 1 (Color online) Overview of optical fiber based VLC network.

coupler (OC), the optical signal is detected and converted to electrical signal to drive LED in each VAP. The received signals are separated from the pre-assigned sub-band [2].

However, signals through the VLC network will display distortion because damage from noise and nonlinearity accumulates in both optical fiber and VLC channel. Geometrically shaping (GS) scheme is proposed to decrease noise and inter-symbol interference on constellation. Constant modulus algorithm (CMA), first proposed by Godard [13], is a classical blind equalization algorithm, and is widely used for signal recovery. Nonetheless, being insensitive to phase of the signal, phase offset remains after CMA equalization.

In this paper, we propose to utilize a machine learning algorithm, the support vector machine (SVM), for phase noise mitigating and signal recovering after CMA in seamless integrated fiber and VLC system, where there are 4 sub-bands representing multiple users in the network. We introduce two designs of GS 8QAM constellation, Diamond and Circular $(7,1)$, and discuss the parameter selection of SVM in detail. Experimental results indicate that at the bandwidth of 320 MHz, overall bitrate of 960 Mbps, system performance can be significantly improved by employing SVM and GS Circular $(7,1)$ scheme. Q-factor increases by up to 11.5 dB, and transmission under 7% forward error correction (FEC) threshold at -2.5 dBm input optical power can be realized when employing Circular $(7,1)$ and SVM.

2 SVM scheme for GS 8QAM constellation

Higher order QAM brings higher spectral efficiency, but meanwhile increases inter-symbol interference, and higher signal-to-noise ratio (SNR) is required. Owing to path loss and divergence angle, the SNR of received signal is limited. GS scheme has been employed for larger minimum Euclidean distance of constellation, so that the influence from noise could be reduced. For GS 8QAM, extensive investigation has been done [14, 15]. In this paper, we compare the two GS 8QAM constellation designs. One is Diamond which is widely used in optical fiber communication system, and the other is Circular $(7,1)$, which is supposed to work best in additive white Gaussian noise (AWGN) channel [15]. Figure 2 is the constellation of the two designs. The minimum Euclidean distance of Circular $(7,1)$ is 0.9277, larger than that of Diamond, which is 0.9144.

SVM as a powerful machine learning method, is usually used to classify two groups of data. Given a set of n training data $(x_i, y_i), i = 1, \ldots, n$, where x_i are feature vectors, and y_i are labels, indicating the classification of data points. The main task of SVM is to find an optimal hyperplane to separate the two

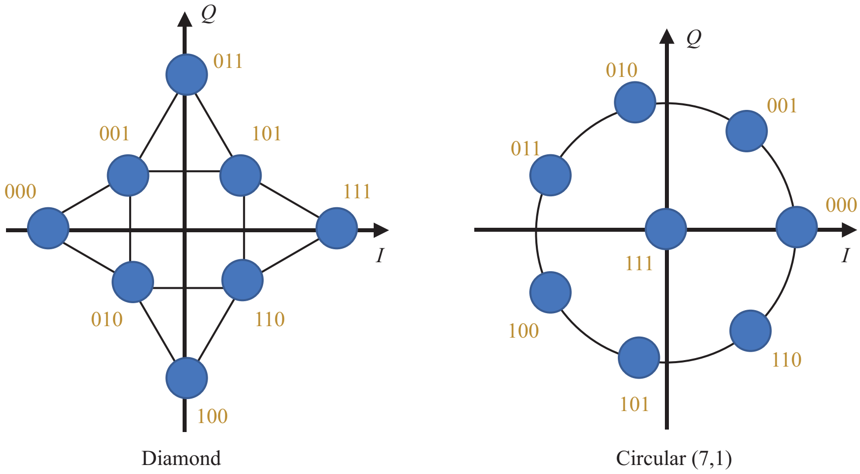

Figure 2 (Color online) Constellations of GS 8QAM Diamond and Circular $(7, 1)$.

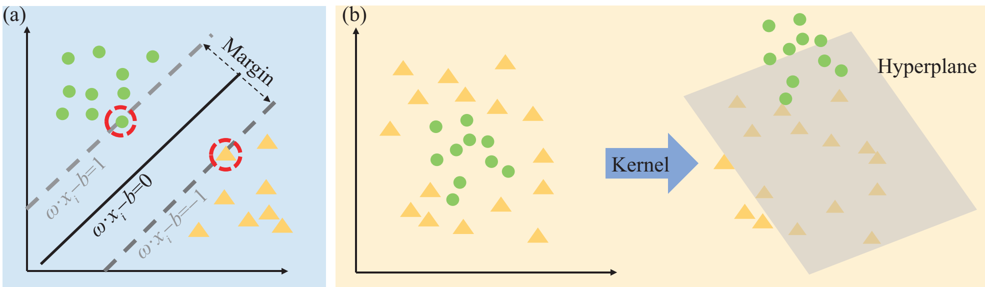

Figure 3 (Color online) (a) Schematic diagram of linear separable SVM and (b) kernel function for linear inseparability.

groups. Any hyperplane in feature space can be expressed as

$$w \cdot x - b = 0. \tag{1}$$

If training data is linear separable, as Figure 3(a) shows, we can find boundary of each group to be parallel to the optimal hyperplane. The classifier can be described as

$$y_i(w \cdot x_i - b) \geqslant 1, \quad i = 1, \ldots, n. \tag{2}$$

The optimal hyperplane meets the condition that the minimum distance from the optimal hyperplane to the nearest points of each side is maximum. The region between the two parallel hyperplanes is called margin, equal to $2/\|w\|$. The nearest points are called support vectors.

For cases where the training data cannot be linearly separated perfectly, to separate training data with a minimal number of errors, some non-negative variables ξ_i are introduced:

$$y_i(w \cdot x_i - b) \geqslant 1 - \xi_i, \quad \xi_i \geqslant 0, \quad i = 1, \ldots, n. \tag{3}$$

To determine w and b of the optimal hyperplane, we should solve the following problem [16]:

$$\min \left[\frac{1}{2}\|w\|^2 + C\sum_{i=1}^{n}\xi_i\right], \quad \text{s.t.} \quad y_i(w \cdot x_i - b) \geqslant 1 - \xi_i, \quad i = 1, \ldots, n. \tag{4}$$

If the training data set is not linearly separable, the kernel trick is proposed to create nonlinear classifier. As Figure 3(b) shows, through this method, original input feature vectors can be mapped to a higher dimensional space and then the data can be linearly separated. The decision function is

$$D(x) = \sum_{i=1}^{n} y_i a_i K(x, x_i) - b, \tag{5}$$

Table 1 Expression of different kernel

Kernel	Expression
Linear	$K(x_1, x_2) = x_1 \cdot x_2^{\mathrm{T}}$
Polynomial	$K(x_1, x_2) = (\gamma(x_1 \cdot x_2^{\mathrm{T}}) + r)^d$
RBF	$K(x_1, x_2) = \exp(-\gamma\|x_1 - x_2\|^2)$
Sigmoid	$K(x_1, x_2) = \tanh(\gamma(x_1, x_2^2) + r)$

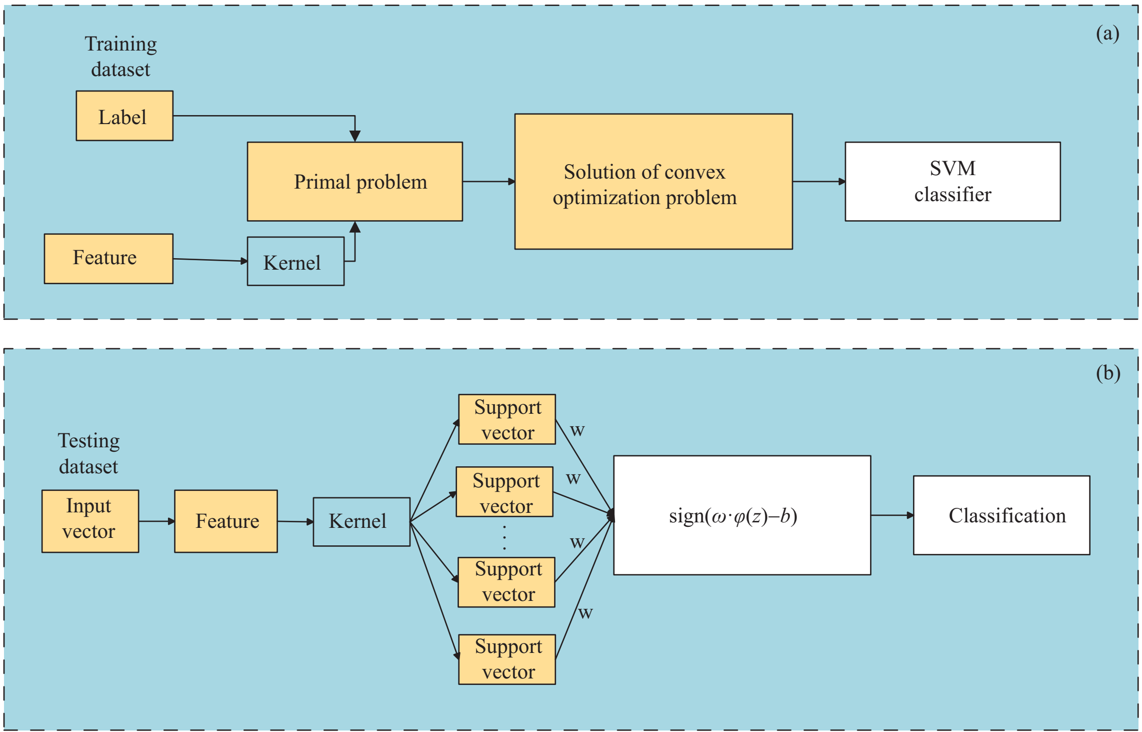

Figure 4 (Color online) Flow chart of SVM. (a) Training phase; (b) testing phase.

where a_i are constant factors and $K(x_1, x_2)$ is kernel function. The choice of kernel function is closely related to the distribution of data points. Common kernel includes polynomial kernel, Radial basis function (RBF) kernel, and sigmoid kernel. Table 1 lists the kernel used in our experiment.

The solution of SVM is a dual quadratic optimization problem. According to [17], any (x_i, y_i) in training data set will meet either $a_i = 0$ or $y_i(w \cdot x_i - b) = 1 - \xi_i$. In the former condition, the point will not make an impact on SVM classifier. In the latter condition, the point is a support vector. Thus, the decision hyperplane only depends on a few support vectors. In summary, the SVM training process is shown in Figure 4(a).

After training, the classification process of the new input data points is shown in Figure 4(b). Firstly, extract eigenvectors from input data, and map them to higher dimensional space through kernel function. Then substitute it into SVM classifier. According to the indicator function:

$$I(x) = \mathrm{sign}(w \cdot \varphi(x) - b), \tag{6}$$

we can predict the classification of the new input sample. When employing SVM to separate data with multi-class, we should firstly build appropriate multi-classifier, so that the multi-class problem can be converted to binary classification. In this experiment, we utilize the SVM multi-class strategy, one versus rest (OVR) in GS 8QAM constellation classification. In the GS 8QAM data OVR SVM training process, we construct one SVM model between each one class and the other seven classes, and finally we get the multi-class classifier with 8 SVM models. This method is obvious and less complicated compared with the strategy one verses one (OVO) [18].

SVM is a powerful machine learning tool, but the computational and storage requirements increase

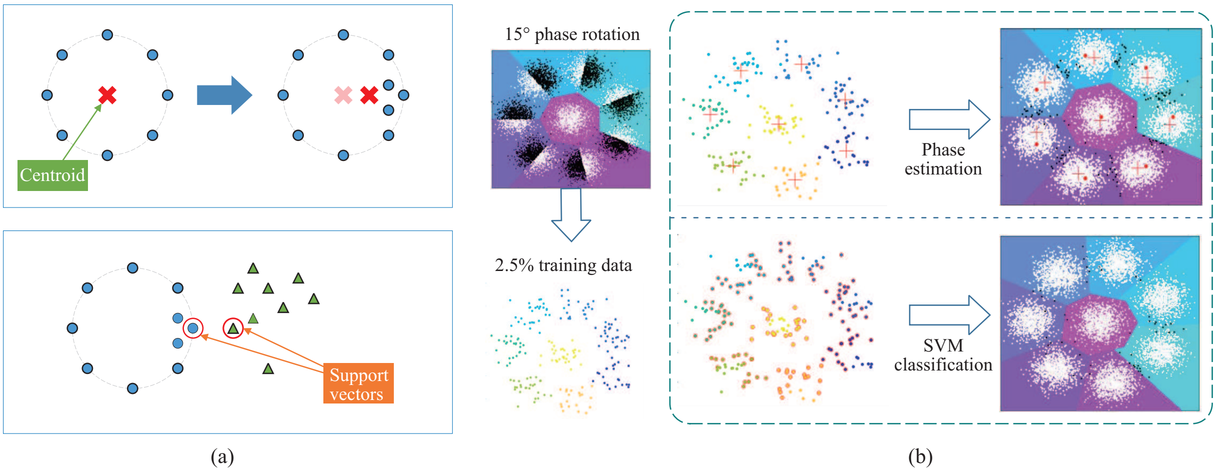

Figure 5 (Color online) (a) Schematic diagram of centroid estimation and SVM classification of biased distribution; (b) simulation results of Circular (7, 1) with 2.5% training data.

rapidly with the number of training vectors. In the training process, the core of an SVM is a quadratic programming problem, separating support vectors from the rest of the training data [19]. The training complexity scales between $\mathrm{O}(dN_t{}^2)$ and $\mathrm{O}(dN_t{}^3)$, where d is the number of features and N_t is the number of training data. The test phase will require $\mathrm{O}(MN_s)$ operations, where M is the number of operations that are required to evaluate the kernel, and N_s is the number of support vectors [20]. Compared with k-means, another machine learning algorithm, the complexity of k-means is $\mathrm{O}(N)$ for an N points dataset [21], the training complexity of SVM seems to be higher. However, in general, SVM only requires a small amount of training data. Furthermore, the complexity of testing, in other words, the classification process depends on few support vectors and M (for linear SVM, the complexity only depends on N_s), but for k-means the complexity is related to the whole dataset. When the testing data is very large, the complexity of k-means will be relatively much higher.

After optical fiber and VLC transmission, the signal may suffer distortion and random phase shift. Thus, the constellation will display dispersion and rotation. Classical demodulation is based on Euclidean distance, of which the result will be profoundly influenced by phase rotation, especially for circular design. To overcome the phase rotation, we can employ a small amount of training data, so that the centroid of each cluster can be estimated (for Circular (7, 1) the phase rotation of central cluster will not be considered). By comparison with the standard position of constellation points, the estimated rotation degree is obtained, and then the constellation can be corrected. However, owing to distortion, the distribution is likely to be unbalanced. Just as the upper part of Figure 5(a) shows, the estimated centroid will be biased, which would lead to severe error. The performance of SVM only depends on several support vectors, the biased centroid almost has no influence on the SVM classifier. In other words, the stability and robustness could be improved.

Let us take Circular (7, 1) as an example. Figure 5(b) is the simulation results of Circular (7, 1). Black points represent error. The constellation displays severe dispersion, and with 15 degree phase rotation, the bit error rate (BER) performance is poor. We split 2.5% of the data as training data equivalently. The upper part of the figure is phase correction based on centroid estimation. Red crosses represent estimated centroid of each cluster. Red points present standard positions of Circular (7, 1) constellation. It can be observed that after phase correction, because of the biased estimated centroid, the constellation is still rotating slightly. After classification based on Euclidean distance, the BER equals to 0.00803. The under part of Figure 5(b) is the process of SVM classification. The points circled in red are support vectors. Compared with the upper classification figure, the number of black points is fewer. The BER equals to 0.00350, under the 7% FEC threshold.

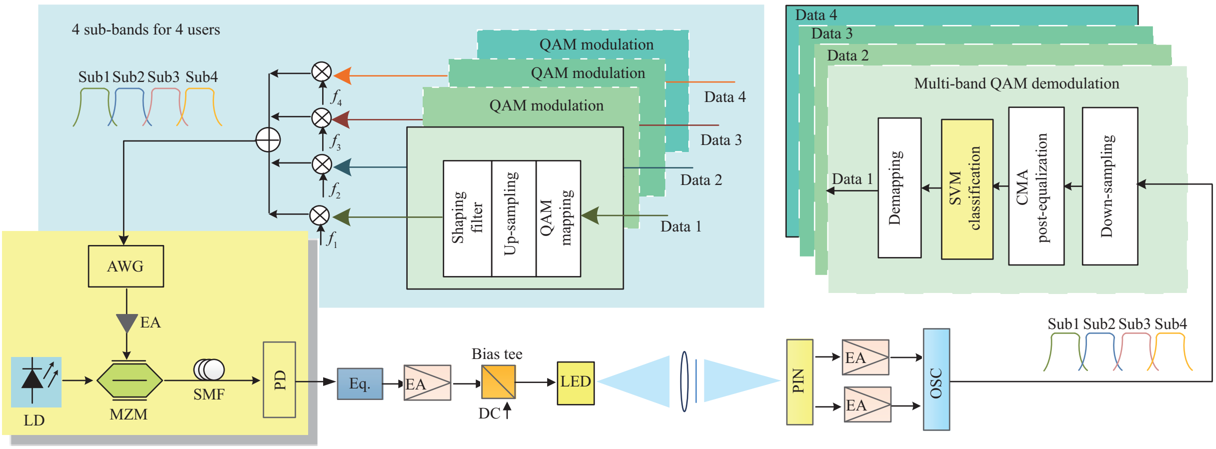

Figure 6 (Color online) Experimental setup of GS 8QAM seamless integrated fiber and VLC system.

3 Experimental setup and results

Figure 6 is the experimental setup of GS 8QAM seamless integrated fiber and VLC system. This system is combined with 2 independent communication system. Firstly, data from 4 users respectively goes through QAM mapping, up-sampling and shaping filter. Then move the signal to four sub-bands. In this process, data of each user are up-converted to different sub-carrier and we obtain real signal. We set the up-sampling rate to 12. The above process is completed by MATLAB. Arbitrary waveform generator (AWG) generates multi-band signal. The bandwidth is fixed at 320 MHz. After amplifier, the signal is input into Mach-Zehnder modulator (MZM), and then modulated with optical carrier produced by laser device (LD). After transmission through 50 m single mode fiber (SMF), the optical signal is converted to electrical signal by photodetector (PD).

Then the electrical signal passes through equalization and electrical amplifier (EA), which helps to overcome the attenuation of LED at high frequency. After coupled with direct current, the electrical signal from optical fiber is loaded to LED, and is transmitted in 1 m free space in the form of intensity. At the VLC receiver, lens and aperture are employed to adjust the receiving power. We also utilize a blue filter to block the yellow component. The PIN photodiode, which contains a p-region, an intrinsic region and an n-region, executes the optical-electrical conversion. Differential output is to reduce common-mode noise. The spectrum of output signal is shown in Figure 7. It is obvious that after VLC transmission, high frequency component of the signal displays attenuation. The signal sampled by oscilloscope (OSC) is separated through down-conversion from different sub-bands, and then the signal recovery process is carried out for each sub-band separately. After down-sampling and CMA equalization, we get signal of which the constellation has preliminarily converged. Then employ SVM for constellation classification to overcome nonlinearity and phase shift in optical fiber and VLC transmission. Finally, perform QAM demapping according to the results of SVM and we could get the original data.

As a supervised machine learning algorithm, performance of SVM is related to various factors such as size of training set, various kernel function, and parameter. In this experiment, we compare four types of kernels which have been introduced in Table 1. In addition, penalty factor C influences model generalization ability, and except linear kernel, the kernel function parameter gamma also affects the accuracy of the model. We employ grid search [22, 23] to find the appropriate ranges of C and gamma for the 3 kernels, just as shown in Figures 8 and 9. Each pair of (C, gamma) is tried, and different colors represent different BER performance at the corresponding C and gamma. The degree of polynomial kernel is 3. The scale of color bar equals to $-\log10(\mathrm{BER})$. The BER results come from the average of 5 training processes in which 20% of the whole data is chosen as training dataset randomly. The redder the color of the grid is, the better the performance exceeds. It is obviously that overall the BER performance of Circular $(7, 1)$ is superior than Diamond. And respectively in each GS design, the BER performance of polynomial is worse than that of the other two kernels.

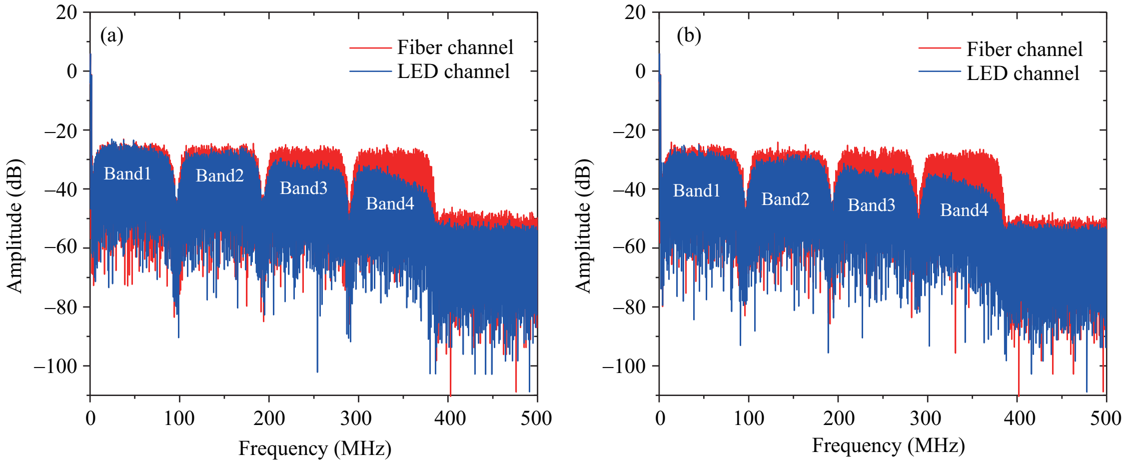

Figure 7 (Color online) Spectrums of Diamond (a) and Circular $(7, 1)$ (b) after optical fiber and LED channel.

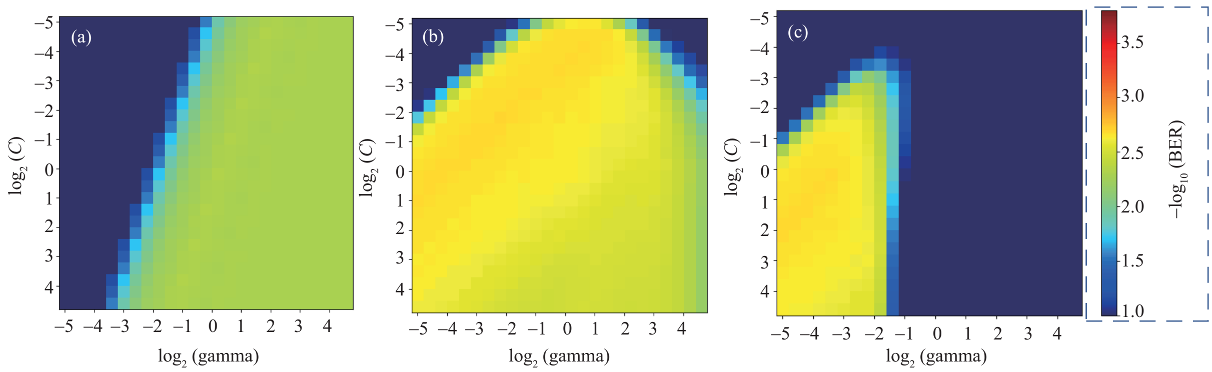

Figure 8 (Color online) Parameters selection of Diamond based on grid research. (a) Poly; (b) RBF; (c) Sigmoid.

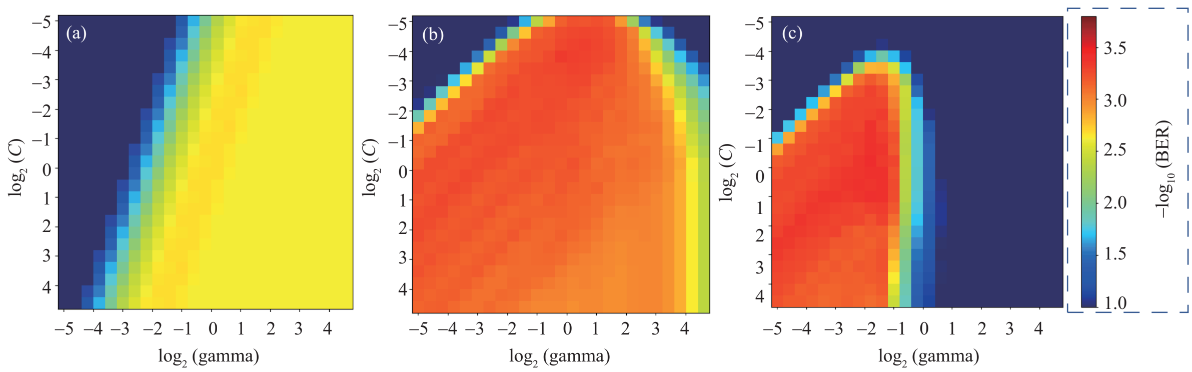

Figure 9 (Color online) Parameters selection of Circular $(7, 1)$ based on grid research. (a) Poly; (b) RBF; (c) Sigmoid.

For better comparison, Figures 10 and 11 are BER results of Diamond and Circular $(7, 1)$ with different kernels versus penalty factor C, respectively, in which for the 3 mentioned kernels we select the position of optimal parameter and make a cross section at the best gamma. It is clear that for the 2 GS constellations, BER tends to decrease with the increase of C. However, because the adaptive intervals of Diamond and Circular $(7, 1)$ are different, and BER curve of different kernel has different descending speed and inflection point. But for each GS constellation, except for polynomial kernel SVM, the best BER performance of the other is considerable close. And in general, Circular $(7, 1)$ has a better BER performance.

According to the discussion above, we can find that the polynomial kernel SVM has a significantly worse performance on the two GS constellation than the other three kernels, and Diamond has a worse

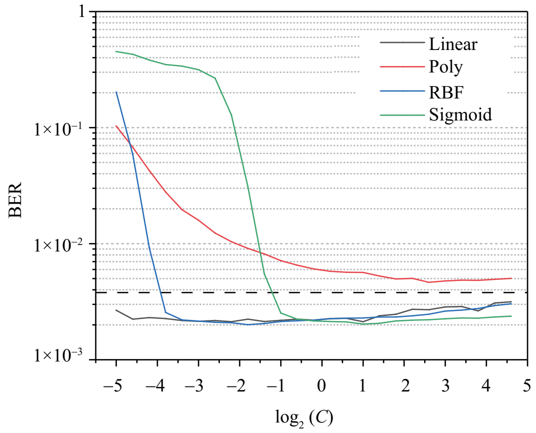

Figure 10 (Color online) BER of Diamond GS 8QAM versus C.

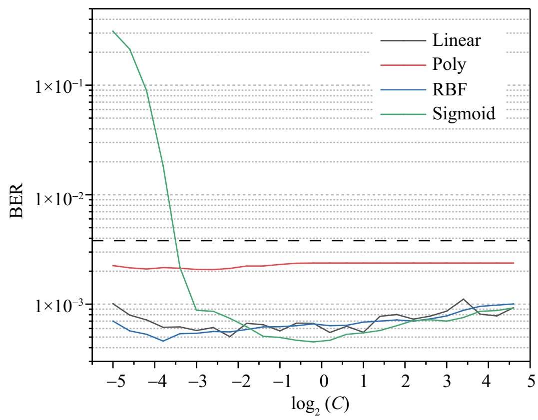

Figure 11 (Color online) BER of Circular $(7, 1)$ GS 8QAM versus C.

Table 2 Expression of different kernels

	Linear	Poly	RBF	Sigmoid
Diamond	$C = 1$	$C = 7.55$, gamma $= 0.05$, degree $= 3$	$C = 0.31$, gamma $= 0.23$	$C = 2.38$, gamma $= 0.05$
Circular	$C = 1$	$C = 0.17$, gamma $= 2.38$, degree $= 3$	$C = 0.07$, gamma $= 1$	$C = 1$, gamma $= 0.42$

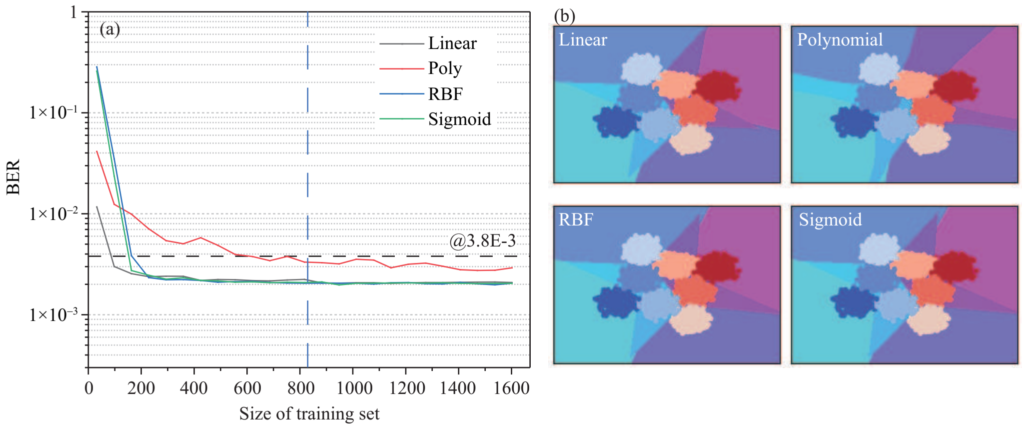

Figure 12 (Color online) (a) BER performance versus size of training data set of Diamond and (b) the classification results of SVM with different kernels.

error performance than Circular $(7, 1)$. Finally, the optimal parameters are selected as Table 2 displays.

To establish efficient machine learning model, besides adjusting the parameters of SVM, size of training set is also critical. On the one hand, if training set is too small, the characteristics of the whole data can not be represented, on the other hand, too large amount of training data will result in waste of resources and increase the cost of transmission. Thus, under the optimum parameters, we change the size of the training set. Figures 12 and 13 are the BER curve averaged by 10 times of random training process. In general, the convergence trend of different kernels is essentially the same. The convergence speed of linear is higher than sigmoid, and higher than RBF. The convergence speed of polynomial kernel is lower and the turning point is not as sharp as the others. The convergent BER of polynomial is obviously higher. Finally, we set the size of training dataset to 10% from the whole data, about 817 samples. The classification results of SVM with different kernel are displayed on the right.

Figure 14 is BER performance of Diamond GS 8QAM versus fiber input optical power. Band1 to Band4 are listed in order. The "w/o" in the figure represents "without". Owing to attenuation at high frequency of LED as shown in Figure 7, the performance of high frequency sub-band becomes worse. We illustrate

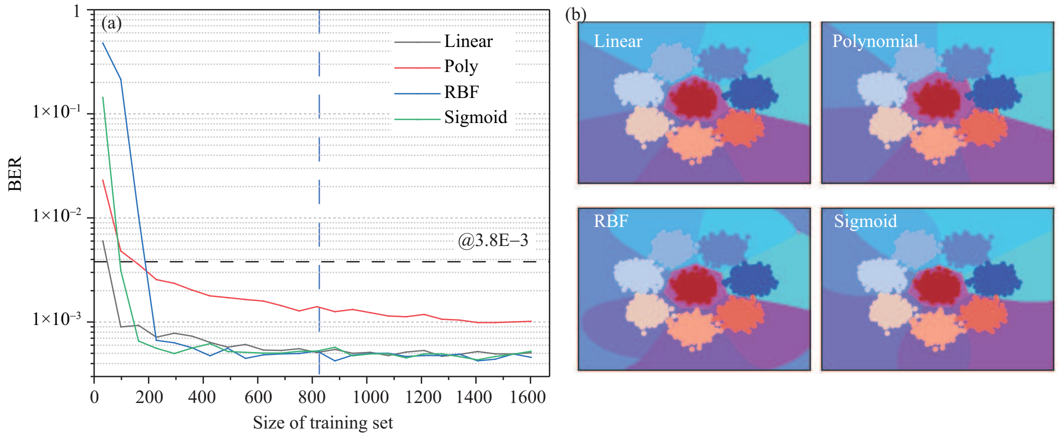

Figure 13 (Color online) (a) BER performance versus size of training data set of Circular (7, 1) and (b) the classification results of SVM with different kernels.

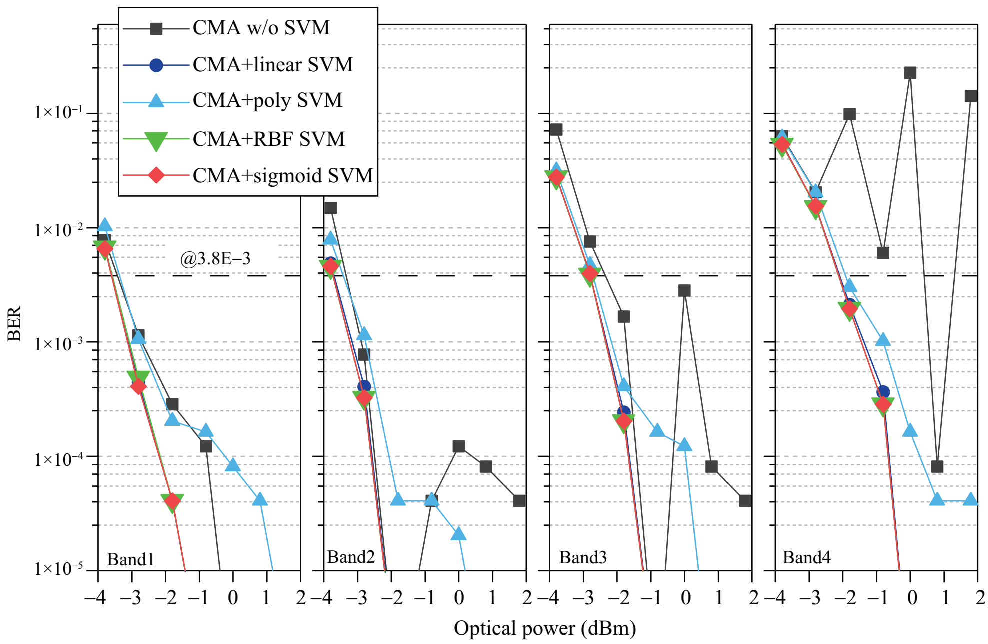

Figure 14 (Color online) BER of 4 bands for Diamond GS 8QAM versus input optical power with different kernel SVMs or without SVM.

the constellation after CMA equalization in Figure 15, and it is clear that at the same optical power, Band4 displays greater dispersion. When employing CMA, the convergence reference modulus is a signal statistical model. Thus the output of the equalizer is insensitive to phase, and phase rotation remains after equalization. As constellation points become dispersed, the inter-symbol interference increases, and BER performance is more susceptible to phase rotation. Furthermore, phase shift appears randomly, and thus BER performance displays severe fluctuation without SVM, especially in Band4. With SVM as input optical power decreases, BER increases and Band4 hits the threshold first. When employing kernel of linear, RBF and sigmoid, BER performance is better than that without SVM, and they have similar results. However, polynomial kernel performs poorly where phase offset is less likely to appear especially at low frequency. In general each coefficient term of the polynomial will not be precisely adjusted, because the process is inefficient. As a result, polynomial kernel is inferior to others.

The first line of Figure 15 shows the distribution of constellation points of Band1 and Band4 of Diamond GS 8QAM after CMA at the maximum and minimum input fiber power respectively. The red points represent the standard positions of GS constellation. It is clear that with the decrease of input

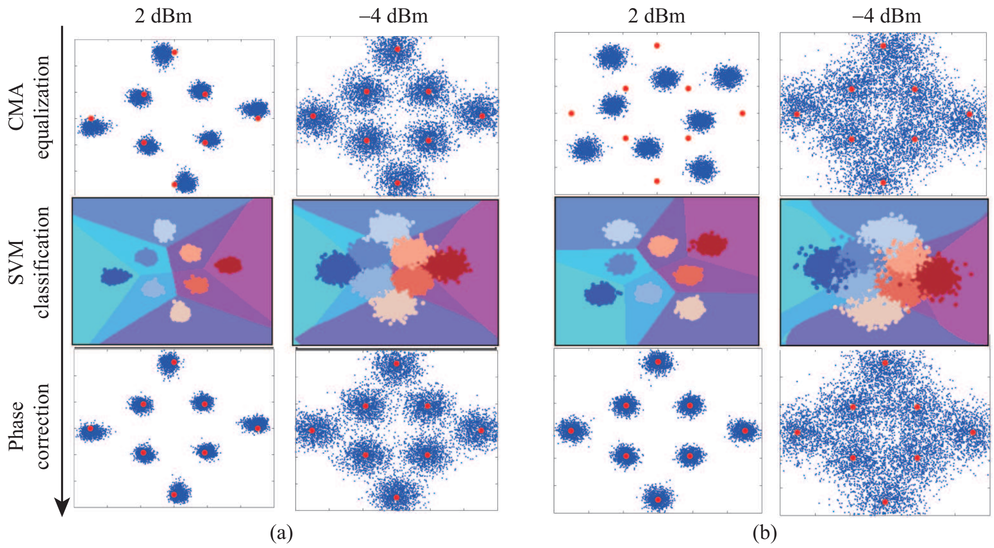

Figure 15 (Color online) Constellation diagrams of Band1 (a) and Band4 (b) at different optical power (2 dBm, −4 dBm) for Diamond after CMA and the classification and phase correction performance of SVM.

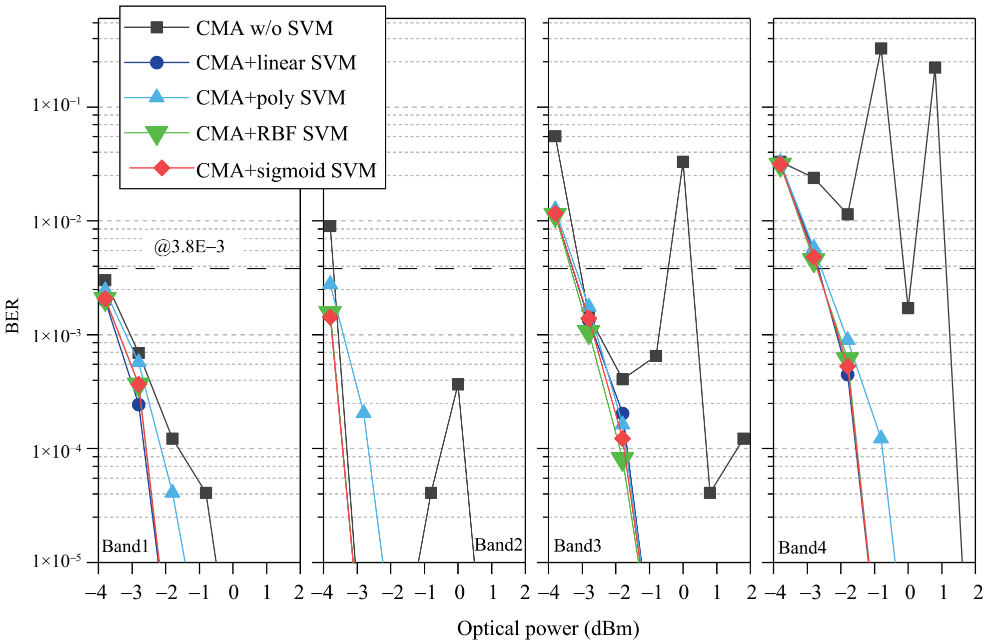

Figure 16 (Color online) BER of 4 bands for Circular (7,1) GS 8QAM versus input optical power with different kernel SVMs or without SVM.

optical power, the distribution of constellation becomes scattered, and in general constellation of Band1 converges better than Band4. The second line is classification of SVM, and we select the results of RBF kernel. In addition, in order to show the classification effect of SVM intuitively, we can estimate the phase rotation degree according to the results of SVM classification. The estimation method has been mentioned in Section 2, but the entire dataset is used for estimation, instead of few training data. And then rotate the constellation after CMA equalization. Finally we obtain the constellation with phase offset corrected. Note that the third line of Figure 15 only serves as a reference of the classification effect of SVM. The decision of constellation has been performed before phase estimation. In multi-band transmission, sub-band with the worst performance determines the capability of the system. For Band4 with low input optical power, owing to severe dispersion of constellation, BER performance gets worse and as Figure 14 shows, has exceeded the 7% FEC threshold at approximately −2 dBm.

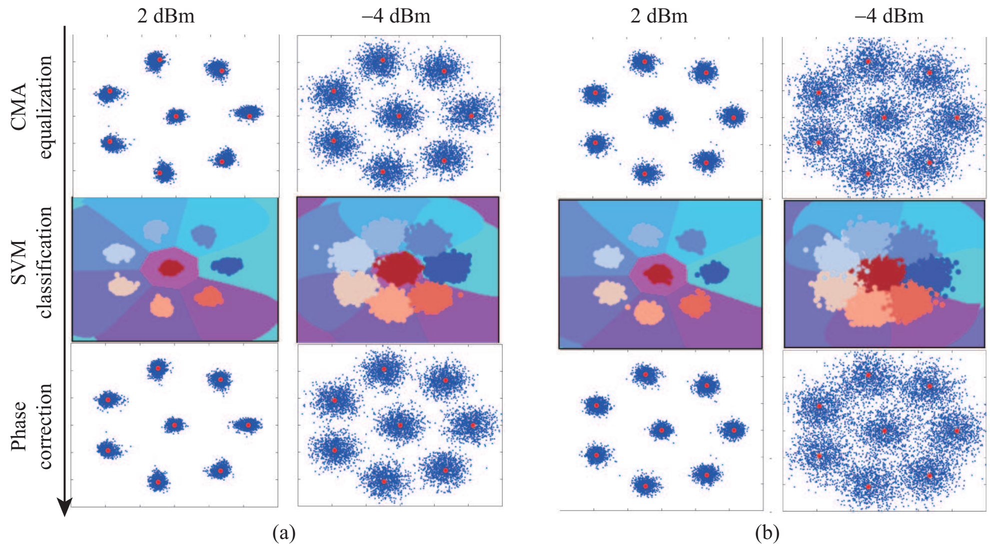

Figure 17 (Color online) Constellation diagrams of Band1 (a) and Band4 (b) at different optical power (2 dBm, −4 dBm) for Circular (7, 1) after CMA and the classification and phase correction performance of SVM.

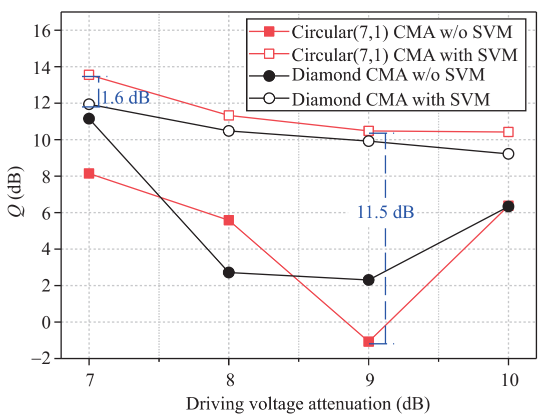

Figure 18 (Color online) Q-factor performance of Diamond and Circular (7, 1) with or without SVM.

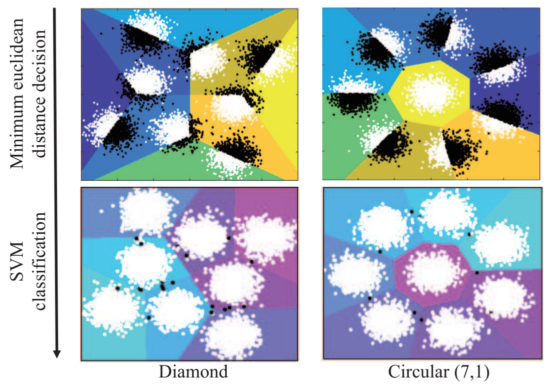

Figure 19 (Color online) Classification respectively based on Euclidean distance and SVM (RBF kernel). Black points represent error.

Figure 16 is the BER performance of Circular (7, 1) GS 8QAM four bands versus optical power. Figure 17 is the constellation of Circular (7, 1). The conclusion is basically consistent to Diamond. However, compared with Diamond, the minimum input optical power that each sub-band can support for Circular (7, 1) is lower, indicating that Circular (7, 1) can ensure a wider dynamic range. BER has exceeded the 7% FEC threshold at approximately −2.5 dBm.

To compare performance of the proposed two GS options, in Figure 18 we analyse Q-factor of Diamond and Circular (7, 1) versus driving voltage attenuation in situations whether SVM is utilized. Results indicate that SVM could eliminate Q-factor fluctuations, and at 9 dB driving voltage attenuation, as Figure 19 shows, the first line is classification based on Euclidean distance and the second line is classification employing SVM. Error (the black points) has been significantly reduced after SVM with RBF kernel because the classification plane could be adjusted according to present constellation distribution. Q-factor of Circular (7, 1) increases by up to 11.5 dB. With the increase of driving voltage attenuation, Q-factor of both Diamond and Circular (7, 1) with SVM decreases. Compared with Diamond, the Q-factor of Circular (7, 1) design can be enhanced approximately 1.6 dBm.

4 Conclusion

VLC network over optical fiber has shown great potential in ultra-high speed indoor wireless communication. To mitigate signal damage accumulated in both optical fiber and VLC channel is worth investigating. In this paper, we demonstrate a 4-band GS 8QAM seamless integrated fiber and VLC system, SVM is employed to mitigate phase offset after CMA equalization. The SVM parameter selection process is discussed in detail. Experimental results show that with the bandwidth of 320 MHz, overall capacity of 960 Mbps, at -2.5 dBm input optical power transmission under 7% FEC threshold can be realized applying Circular $(7, 1)$ GS 8QAM and SVM, and Q-factor increases by up to 11.5 dB.

Acknowledgements This work was partially supported by National Key Research and Development Program of China (Grant No. 2017YFB0403603) and National Natural Science Foundation of China (Grant No. 61571133).

References

1 Chi N, Haas H, Kavehrad M, et al. Visible light communications: demand factors, benefits and opportunities [guest editorial]. IEEE Wirel Commun, 2015, 22: 5–7
2 Wang Y, Chi N, Wang Y, et al. Network architecture of a high-speed visible light communication local area network. IEEE Photon Technol Lett, 2015, 27: 197–200
3 Chow C W, Yeh C H, Liu Y, et al. Network architecture of bidirectional visible light communication and passive optical network. IEEE Photon J, 2016, 8: 1–7
4 Komine T, Nakagawa M. Integrated system of white LED visible-light communication and power-line communication. IEEE Trans Consumer Electron, 2003, 49: 71–79
5 Langer K D, Grubor J, Bouchet O, et al. Optical wireless communications for broadband access in home area networks. In: Proceedings of 2008 10th Anniversary International Conference on Transparent Optical Networks, 2008. 149–154
6 Tsonev D, Videv S, Haas H. Light fidelity (Li-Fi): towards all-optical networking. In: Proceedings of the SPIE, 2013
7 Chen C Y, Wu P Y, Lu H H, et al. Bidirectional 16-QAM OFDM in-building network over SMF and free-space VLC transport. Opt Lett, 2013, 38: 2345
8 Chi N, Zhou Y, Liang S, et al. Enabling technologies for high-speed visible light communication employing CAP modulation. J Lightw Technol, 2018, 36: 510–518
9 Chi N, Zhao Y, Shi M, et al. Gaussian kernel-aided deep neural network equalizer utilized in underwater PAM8 visible light communication system. Opt Express, 2018, 26: 26700
10 Chi N, Shi M. Advanced modulation formats for underwater visible light communications. Chin Opt Lett, 2018, 16: 120603
11 Niu W, Ha Y, Chi N. Novel phase estimation scheme based on support vector machine for multiband-CAP visible light communication system. In: Proceedings of 2018 Asia Communications and Photonics Conference, 2018. 1–3
12 Haigh P A, Chvojka P, Zvanovec S, et al. Experimental verification of visible light communications based on multi-band CAP modulation. In: Proceedings of Optical Fiber Communication Conference, 2015
13 Godard D. Self-recovering equalization and carrier tracking in two-dimensional data communication systems. IEEE Trans Commun, 1980, 28: 1867–1875
14 Zhao J, Qin C, Zhang M, et al. Investigation on performance of special-shaped 8-quadrature amplitude modulation constellations applied in visible light communication. Photon Res, 2016, 4: 249
15 Thomas C, Weidner M, Durrani S. Digital amplitude-phase keying with M-ary alphabets. IEEE Trans Commun, 1974, 22: 168–180
16 Press W H, Teukolsky S A, Vetterling W T, et al. The Art of Scientific Computing. 3rd ed. Cambridge: Cambridge University Press, 2011. 883–886
17 Cortes C, Vapnik V. Support-vector networks. Mach Learn, 1995, 20: 273–297
18 Hsu C W, Lin C J. A comparison of methods for multiclass support vector machines. IEEE Trans Neural Netw, 2002, 13: 415–425
19 Graf H P, Cosatto E, Bottou L, et al. Parallel support vector machines: the cascade svm. In: Proceedings of Advances in Neural Information Processing Systems, 2005. 521–528
20 Burges C J C. A tutorial on support vector machines for pattern recognition. Data Min Knowl Discov, 1998, 2: 121–167
21 Nazeer K A, Sebastian M P. Improving the accuracy and efficiency of the k-means clustering algorithm. In: Proceedings of the World Congress on Engineering. London: Association of Engineers, 2009. 1–3
22 Hsu C W, Chang C C, Lin C J. A Practical Guide to Support Vector Classification. Technical Report, Department of Computer Science, National Taiwan University. 2003
23 Wang D, Zhang M, Li Z, et al. Optimized SVM-based decision processor for 16QAM coherent optical systems to mitigate NLPN. In: Proceedings of Asia Communications and Photonics Conference, 2015